Review **Open Access**

Vladislav A. Sadykov, Vitaliy S. Muzykantov, Nikita F. Yeremeev*, Vladimir V. Pelipenko, Ekaterina M. Sadovskaya, Alexey S. Bobin, Yulia E. Fedorova, Daiana G. Amanbaeva, Alevtina L. Smirnova

Solid Oxide Fuel Cell Cathodes: Importance of Chemical Composition and Morphology

DOI 10.1515/cse-2015-0004
Received December 31, 2014 accepted October 25, 2015

Abstract: The main aspects of the cathode materials morphology for Intermediate Temperature Solid Oxide Fuel Cells (IT SOFC) are considered in this paper. The approaches for estimation of their basic properties, e.g. oxygen mobility and surface reactivity, are described and the results of different techniques (e.g. weight and conductivity relaxation, oxygen isotope exchange) application for studies of powders and dense ceramic materials are compared. The Ruddlesden-Popper type phases (e.g. Pr_2NiO_4) provide enhanced oxygen mobility due to cooperative mechanism of oxygen interstitial migration. For perovskites, the oxygen mobility is increased by doping, which generates oxygen vacancies or decreases metal-oxygen bond strength. Non-additive increasing of the oxygen diffusion coefficients found that for perovskite-fluorite nanocomposites, it can be explained by the fast oxygen migration along perovskite-fluorite interfaces. Functionally graded nanocomposite cathodes provide the highest power density, the lowest area specific polarization resistance, and the best stability to degradation caused by the surface layer carbonization/hydroxylation, thus being the most promising for thin film IT SOFC design.

***Corresponding author: Nikita F. Yeremeev,** Boreskov Institute of Catalysis, 630090 Novosibirsk, Russian Federation, E-mail: yeremeev21@gmail.com
Vladislav A. Sadykov, Vitaliy S. Muzykantov, Vladimir V. Pelipenko, Ekaterina M. Sadovskaya, Alexey S. Bobin Yulia E. Fedorova , Daiana G. Amanbaeva, Boreskov Institute of Catalysis, 630090 Novosibirsk, Russian Federation
Vladislav A. Sadykov, Novosibirsk State University, 630090 Novosibirsk, Russian Federation
Yulia E. Fedorova, Novosibirsk State Pedagogical University, 630126 Novosibirsk, Russian Federation
Daiana G. Amanbaeva, Novosibirsk State Technical University, 630073 Novosibirsk, Russian Federation
Alevtina L. Smirnova, South Dakota School of Mines & Technology, SD 57701, Rapid City, USA

Keywords: SOFC, Cathodes, Perovskites, Fluorites, Composites, Isotope exchange, Relaxation studies, Oxygen mobility, Power density

1 Introduction

In a solid oxide fuel cell (SOFC), the basic function of cathodes is the reduction of O_2 molecules into O^{2-} ions and their transport to the electrolyte [1]. The efficient performance of the cathodes, especially for SOFC operating in the intermediate temperature (IT) range, could be provided only by meeting the requirements of high electronic and ionic conductivity, high catalytic activity in dissociation of O_2 molecules, and chemical stability in air and thermochemical compatibility with electrolyte [2,3]. For the practical applications, cathodes should be manufactured from relatively inexpensive materials using simple procedures. The YSZ-supported LSM or LSM/YSZ composites are the state-of-the-art cathode materials for high-temperature SOFCs [1-3]. For IT SOFC, cathodes comprised of complex perovskite-like oxides (e.g. with Co, Ni, Cu, Mn, and Fe cations in the B sublattice) need additional efforts for their practical application. This is due to a variety of solid electrolytes, their interaction with cathode materials, and long-term degradation because of Cr poisoning or accumulation of carbonates in the surface layers [4-11]. The mixed ionic-electronic conducting nanocomposites comprised of perovskites and electrolytes are considered as the most promising cathode materials for IT SOFC due to better matching of the thermal expansion coefficients (TECs), improved microstructure and stability, high surface reactivity, and enhanced oxygen mobility [12-20]. However, their tailor-made microstructural and morphological design needs innovative solutions due to the interaction between perovskite and electrolyte domains. This design should be based on elucidation of atomic-scale factors

controlling kinetics of elementary steps of oxygen activation on the surface sites, incorporation of oxygen atoms into the lattice, and migration. For nanocrystalline/nanocomposite oxide materials, these problems are still in question despite application of numerous advanced techniques [21-38], as well as theoretical methods [39-41] for characterization of the surface reactivity and bulk oxygen diffusion. Uncertainty in data analysis is caused by variation of the surface structure and composition of the complex oxide materials as a function of their sintering temperature, anisotropy of the oxygen diffusion, and appearance of channels of fast oxygen migration along grain boundaries [42-48]. This uncertainty is complicated by the fact that known models of the cathode performance are usually based on the assumption of uniform surface and only one-channel of oxygen diffusion in the bulk [3,49-51].

The main aspects of these problems are reviewed with a special attention to the effect of the cathode materials composition and microstructure (especially for perovskite-fluorite interfaces) on the surface reactivity and lattice oxygen mobility.

2 Basic Types of Cathode Materials and Their Functional Properties

2.1 Perovskites and Perovskite-like Structures

2.1.1 Perovskites

Perovskites comprise a large class of complex oxides. Perovskite structure has an ideal formula ABO_3 and consists of large-size 12-coordinated cations at the A-site and small-size 6-coordinated cations at the B-site. Perovskite compounds with different combinations of cations in the A and B sites, e.g., I-V, II-IV or III-III and their more complex combinations are known. A remarkable feature of perovskites is a possibility of cationic substitutions in both A and B-sites over a wide concentration range. Among perovskites, the most studied systems as cathode materials are based on manganites, ferrites, nickelates, and cobaltites of lanthanides (e.g. A = La, Pr, and Sm) with a variety of substitution in A and B sublattices [1-3]. In the SOFC operation temperature range of 600–800°C, these oxides possess a high total conductivity (10–1000 S cm^{-1}) of either metallic or semiconductor type [19,51]. The highest conductivity is found for $La_{1-x}Sr_xCoO_{3-d}$ (LSC) or $SrCoO_3$ [51]. However, some Pr-containing perovskites such as $PrNi_{0.6}Co_{0.4}O_3$ are reported to demonstrate specific conductivity exceeding 1000 S cm^{-1} at 1000 K [19]. The conductivity of manganites is metallic and lower compared to cobaltites, and conductivity decreases as you dope with Co and Ni. The conduction mechanism changes from a metallic type to a localized hopping of charge carriers between the Mn^{3+} and Mn^{4+} sites causing the conductivity (σT) to increase with temperature [51].

During the oxygen molecules activation, the activity of surface sites characterized by the specific rate of oxygen heteroexchange (k_{ex}) is comparable for different ABO_3 perovskites with a variation within two orders of magnitude (~10^{-8}–10^{-6} cm s^{-1} at 700°C), and increases with decreasing Me-O bond strength [14-18]. As a result, cobaltites usually demonstrate a higher specific surface reactivity due to a lower Me-O bond strength [18]. For the same perovskite composition, the specific rate of oxygen heteroexchange depends on the route of synthesis and the calcination temperature causing a variation of the surface composition, formation of different phases, and changes in the structure and morphology [18]. On the contrary, the range of oxygen mobility, characterized by the oxygen self-diffusion coefficient (D^*), is very broad changing within 9 orders of magnitude at 1000 K (e.g. ~10^{-6} cm^2 s^{-1} for $PrBaCo_2O_{5+\delta}$ [45], ~10^{-8} cm^2 s^{-1} for $La_{0.5}Sr_{0.5}CoO_3$, $La_{0.6}Sr_{0.4}Co_{0.2}Fe_{0.8}O_3$, $La_{0.6}Sr_{0.4}Co_{0.98}Ni_{0.02}O_3$ [35,37,38], and ~10^{-15} cm^2 s^{-1} for $La_{0.8}Sr_{0.2}MnO_3$ [30]).

In general, the oxygen diffusion in a cubic perovskite structure occurs by hopping of oxygen anions into the neighboring oxygen vacancies along a curved path with a saddle point configuration corresponding to the oxygen anion pass through a triangle comprised of one B and two A cations [39]. For $La_{0.8}Sr_{0.2}MnO_3$ (LSM), a low oxygen mobility is explained by the defect structure of manganites favoring cation vacancies at the oxygen excess typical for these perovskites in contact with air [18,51]. As a cathode material, LSM mainly operates via surface path, including dissociation of O_2 molecules at surface sites and migration of oxygen atoms to $La_{0.8}Sr_{0.2}MnO_3$ – $Zr_{0.84}Y_{0.16}O_2$ (LSM/YSZ) interface followed by oxide ions incorporation into the surface YSZ vacancies [3]. At a moderate to high cathodic overpotentials, LSM becomes sufficiently reduced and opens up a parallel bulk transport path near the three-phase boundary like the perovskite mixed ionic-electronic conductors.

In lanthanides based on cobaltites and nickelates, substitution of Ln^{3+} for Sr^{2+} increases oxygen self-diffusion coefficients due to formation of oxygen vacancies as required by the charge balance. The correlation between the thermal expansion and the oxide ion transport in mixed conducting perovskite-type oxides, such as $SrCoO_3$ possessing the highest oxygen mobility, makes them

chemically instable and incompatible with majority of electrolytes [e.g. $Zr_{0.84}Y_{0.16}O_2$ (YSZ), $Ce_{1-x}Y_xO_2$ (GDC), and $Zr_{1-x}Sc_xO_2$ (ScSZ)]. Hence, materials with the intermediate oxygen mobility (e.g. LSF, LSCF, and LFN) are often used [51-53]. However, due to a high reactivity with doped zirconia electrolytes, these perovskites are usually used in combination with doped ceria (e.g. GDC and SDC) either as a main electrolyte or as a buffer layer between the electrolyte and the cathode [51].

2.1.2 Ruddlesden-Popper phases

The Ruddlesden-Popper (R-P) phases with a general composition $AO(ABO_3)_n$ form layered structures by stacking *n* layers with a perovskite structure and AO layer with a NaCl structure. Mainly, nickelates of La, Pr, and Nd, with a partial substitution of Ln for Sr and Ni for Co, Cu, and Fe, were studied as cathode materials [9,10,51]. In the intermediate temperature range, their total specific conductivity (of semiconductor or metallic type) varies between 10 and 100 S cm^{-1}, which is sufficient for the SOFC cathode applications [1,51]. The thermal expansion coefficient of La_2NiO_4 is 12.4×10^{-6} K^{-1} [9], which matches that of Sm-doped ceria (SDC). Oxygen mobility in these systems is provided by interstitial oxide ions located in the A_2O_2 layers, so it is highly anisotropic [40,41,46]. Incorporation of oxygen into interstitial positions strongly distorts BO_6 octahedra, and their pronounced relaxation accompanies oxide ion diffusion along the sinusoidal pathway involving both regular and interstitial positions. It proceeds via the promotion of an apical oxygen ion into the adjacent interstitial site leaving a vacant site in one of the NiO_6 octahedra. This vacant site is then filled by a second neighbouring interstitial oxygen [41]. As the result, the oxygen diffusion coefficients are usually higher for R-P phases in comparison to perovskites, with oxygen self-diffusion coefficient up to 10^{-7} cm^2 s^{-1} at 1000 K and chemical diffusion coefficient up to 10^{-4} cm^2 s^{-1} [32-33,46]. The rate of the surface reaction is also high due to the structure specificity [40] with the surface chemical exchange coefficient (k_{chem}) up to 10^{-3} cm s^{-1} at 1000 K for sintered ceramic samples [47]. The most active sites for O_2 dissociation are located at rough faces with more disordered atomic structure, which are formed during high-temperature sintering. Partial substitution of Ni for Co only slightly affects the oxygen diffusion, while significantly increasing the values of k_{chem} [33]. Additional advantage of R-P phases is in their high oxygen mobility in absence of alkaline earth cations. For $Pr_2NiO_{4+\delta}$, the best SOFC performance with YSZ electrolyte was obtained when using a GDC barrier layer [10]. This was explained by a two orders of magnitude higher area specific resistance (ASR) of $Pr_2NiO_{4+\delta}$ cathode layer on YSZ electrolyte due to a chemical interaction of R-P $Pr_2NiO_{4+\delta}$ phase with YSZ [54].

2.2 Composites

The composites of perovskites or R-P type oxides with electrolytes are attractive as cathode materials for SOFCs because they provide a higher area of the Triple Phase Boundary (TPB), increased oxide ion conductivity and enhanced rate of surface reactions [12-20]. As a result, the area-specific polarization resistance of cathodes is decreased. In the case of porous GDC interlayer between YSZ and perovskite, the composites can be formed due to incorporation of perovskite particles into the pores of GDC layer [18]. While the LSM-YSZ or LSM-ScCeSZ composites are the most studied [1,2,14,18,51], numerous studies were carried out with LSGM-LSM [20], LSCF-GDC [13, 18, 25], LSFN-GDC [15,17,18], $PrNi_{0.6}Co_{0.4}O_3$–$Ce_{0.8}Sm_{0.2}O_{1.9}$ [19] and other systems.

The important problem of the composite cathode materials is in controlling their microstructure due to its strong effect on the performance [13] and interaction between perovskite and electrolyte domains, which results in redistribution of cations [14-18]. This interaction leading to formation of new phases, deterioration of transport properties, and decrease in surface reactivity [51] was demonstrated for LSFN-ScCeSZ composite sintered at excessively high temperatures [55]. The traditional approaches such as mixing and ball milling of commercial perovskite and fluorite powders [25] could hardly provide reliable control of the microstructure. Advanced methods of nanocomposite synthesis such as spray pyrolysis of the mixed nitrate solutions [56], one-pot polymeric precursor (Pechini) route [57], ultrasonic dispersion of the mixture of nanocrystalline powders in organic solvents with addition of surfactants [14-18], and mechanical activation [58] capable of providing uniform spatial distribution of domains of both phases in nanocomposites are apparently attractive for tailor-made design of nanocomposites with a required microstructure.

2.3 Characterization of the oxygen diffusion and surface reactivity

2.3.1 Definitions

The ionic conductivity (σ_i) and diffusion coefficient (D) are correlated via the Nernst-Einstein equation

$$D = f\frac{\sigma_i k_B T}{q^2 C}, \quad (1)$$

where k_B is Boltzmann constant, q and C are ionic charge and concentration respectively, and f is correlation factor (~1). The diffusion coefficient is defined by ionic mobility mechanism and may be expressed in terms of ion hopping. It is evident that the presence of oxygen vacancies is necessary for the oxygen diffusion. The oxygen surface reactivity expressed by the exchange coefficient (k) is another important kinetic parameter characterizing the rate of oxygen transport from the gas phase into complex metal oxides. It is a measure of the rate of the neutral oxygen flux (J_O) crossing the surface of the oxide.

For oxygen diffusion under the gradient of its chemical potential (m), the chemical diffusion coefficient (D_{chem}) is used instead of D^*. A relation between the oxygen isotope diffusion parameters and the chemical diffusion parameters is given by the equation $D_{chem} = g\,D^*/H_R$, where H_R is the Haven ratio (~1) [28], and g – thermodynamic factor. The thermodynamic factor can be obtained from TGA measurements of nonstoichiometry δ as a function of oxygen partial pressure p_{O_2}: [23-25,28]

$$\gamma = -\frac{1}{2}\frac{\partial \ln p_{O_2}}{\partial \ln \delta} \tag{2}$$

2.3.2 Experimental Techniques for Investigation of the Transport Properties and Surface Reactivity

For dense ceramics, parameters characterizing their transport properties (e.g. electronic and ionic conductivity, oxygen tracer diffusion, and chemical diffusion) and surface reactivity can be studied by several methods, such as impedance spectroscopy [45], coulometric titration [23], ^{18}O tracer profile analysis by secondary ion mass spectrometry (SIMS) [48], $^{18}O/^{16}O$ isotope exchange kinetics by gas-phase analysis of the isotope composition [58], or the change in weight of an oxide during the isotope exchange with a microbalance [38]. Impedance spectroscopy includes conductivity measurements in an active current with varying frequency and separating the real and imaginary parts of complex electrical impedance, which allows distinction between various types of conductivity, including ionic conductivity [45]. Coulometric titration in the potentiostatic mode is performed by step-wise electromotive force change and monitoring the current decay, while potentiostatic step involves changing the oxygen partial pressure inside the cell with the chemical diffusion allowing the adaption of the oxygen stoichiometry to the oxygen partial pressure [23]. Relaxation methods involving measurements of conductivity or mass change after a sudden change of pO_2 are also known [26,28,36]. For powder samples, the oxygen isotope heteroexchange with mass-spectroscopic control of the isotope gas-phase in static or flow modes is a well-established technique allowing estimation of the main parameters of the surface reaction steps and surface/bulk oxygen diffusion [14,18,49].

2.3.2.1 Electrical conductivity relaxation (ECR) and weight relaxation methods.

ECR method is rather simple, it does not require expensive equipment and it provides high precision in the determination of the oxygen chemical diffusion and surface exchange coefficients in mixed ionic-electronic conductors. When a mixed ionic-electronic conductor (i.e. $La_{1-x}Sr_xBO_{3-\delta}$) is subjected to an oxygen chemical potential gradient, a chemical diffusion of oxygen ions lowers the gradient (or the diffusion of oxygen vacancies in the opposite direction) and a redistribution of electronic carriers takes place. The defect concentration gradient can be determined by ambipolar diffusion of $V_O^{\bullet\bullet}$ and e' (in parallel direction) or $h^{\bullet}$ (in counter direction for a p-type regime). The effect of the surface reaction should be considered as the boundary condition for obtaining a solution to the Fick's second law:

$$\frac{dC_h}{dt} = D_{chem}\hat{\Delta}C_h, \tag{3}$$

where C_h is hole concentration, D_{chem} is chemical diffusion coefficient, $\hat{\Delta}$ is Laplace operator. Then, an analytical solution may be obtained in the approximation that the surface reaction kinetics is linear with respect to the oxygen concentration at the surface.

2.3.2.2 Oxygen isotope exchange

For dense ceramics, such technique as secondary ion mass spectrometry (SIMS) depth profiling is applied. The sample with a natural oxygen isotope composition is first kept at the operation temperature under contact with oxygen enriched with the ^{18}O isotope for a fixed time. For powder samples, the mass-spectroscopic (MS) analysis of the gas phase during isotope exchange is used for characterization of both the surface reaction and the oxygen diffusion in the bulk. In the analysis of O_2 isotopic composition three routes of exchange must be taken into account [48]: redistribution between the molecules of the gas phase and the isotopic heteroexchange between the gas phase and the surface oxygen atoms of a solid oxide $(O)_S$:

$$^{18}O_2 + {}^{16}O_2 = 2\,{}^{18}O^{16}O \quad (I)$$
$$^{18}O_2 + (^{16}O)_S = {}^{18}O^{16}O + (^{18}O)_S \quad (II)$$
$$^{18}O_2 + 2\,(^{16}O)_S = {}^{16}O_2 + 2\,(^{18}O)_S \quad (III)$$

The distribution of molecules $^{18}O_i{}^{16}O_{2-i}$ (i = 0, 1, 2), characterized by their molar fractions (x_i), is determined by two independent isotope composition variables, since $x_0 + x_1 + x_2 = 1$. The ^{18}O fraction of the oxygen gas, $\alpha = 0.5x_1 + x_2$, is usually selected as the first variable, while the second independent variable can be chosen as a fraction of any of the oxygen molecules, i.e. $^{18}O\,{}^{16}O$ (x_1). With these variables, the redistribution of the isotopes in the system is described by isotope-kinetic equations [48]. For a complete description of the isotope redistribution, the differential equations reflecting the isotope transfer in the solid phase should be added to the system. In the case of equivalent exchangeable oxygen atoms (N_e), the time dependence of the gas phase isotopic fraction, $\alpha(t)$, is well described by an exponential function. The complete system of equations can be used to estimate the self-diffusion coefficient for oxygen in the bulk of the solid oxide. For this purpose, a numerical analysis of the time dependence of the isotope variables, which corresponds to the solution of the inverse problem of the system of equations, was carried out through the minimization of the objective functional [18,59].

Temperature programmed isotopic exchange experiments (TPIEs) also allow a semi-quantitative characterisation of the oxygen mobility. Thus, the depth of the isotope penetration from the gas phase into the oxide in the course of TPIE can be characterized by the value N_X determined by the isotope balance equation in the closed system. This quantity varying from 0 to the total number of exchangeable atoms is used as the measure of the number of exchanged oxygen atoms in the solid oxide phase [18,48].

2.3.3 Powder Sample Analysis

Oxygen isotope exchange is the main technique, which can be applied to powder samples [14-18]. Typical results for temperature dependences of specific rates of oxygen heteroexchange for different perovskites are given in Figs. 1 and 2. In general, the specific rates of exchange are comparable for manganites, nickelates, and cobaltites, which is explained by rather close bonding energy of Me-O terminal oxygen species (~60–80 kcal mol^{-1}) for transition metal cations on the surfaces of perovskite domains. In agreement with the data for dense samples [32], $Pr_{2-x}NiO_{4+\delta}$ demonstrates a high rate of the surface reaction, which can be explained by the positive role of the Pr^{3+}/Pr^{4+} redox pairs. The perovskite-fluorite nanocomposites also provide a comparable rate of the isotope exchange increasing with the temperature of sintering (Figs. 3 and 4) [59]. According to the detailed studies of the surface composition and real/defect structure of these nanocomposites [14-18], this effect is explained by migration of transition metal cations on the surface of electrolyte domains creating new active sites [18]. A powder sample screening can be performed by measuring the oxygen mobility by the dynamic extent of exchange. In agreement with the results for the dense materials, this parameter varies in a broad range and has a tendency to increase with the sintering temperature for perovskites, GDC, and perovskite-GDC nanocomposite (Figs. 5 and 6).

For LSFN-GDC nanocomposite sintered at temperatures up to 1200°C, the oxygen mobility is non-additively increased

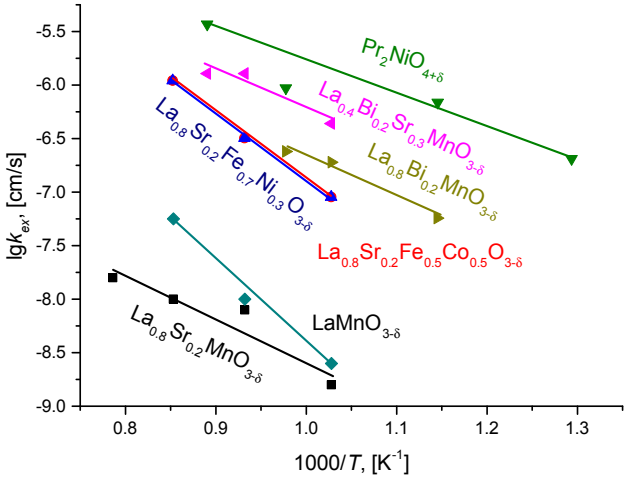

Figure 1. Typical temperature dependencies of specific rates of oxygen heteroexchange for perovskite-like mixed oxides.

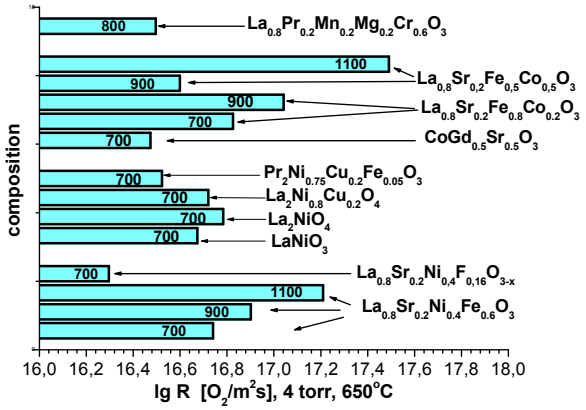

Figure 2. Specific rate of the oxygen heteroexchange at 650°C and 4 Torr O_2 versus samples composition and sintering temperature.

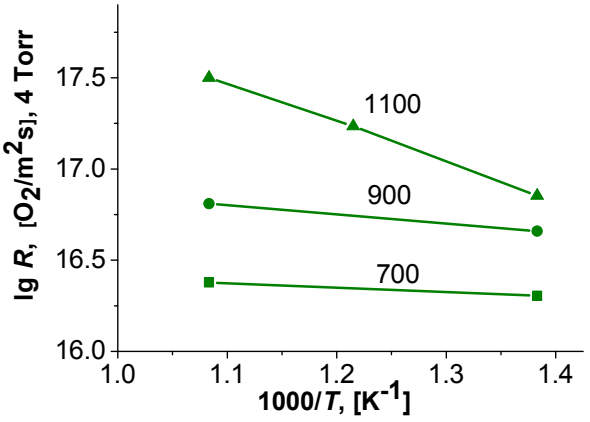

Figure 3. Typical temperature dependencies of specific rates of oxygen heteroexchange for $LSFN_{0.4}$-GDC nanocomposites sintered at 700–1100°C.

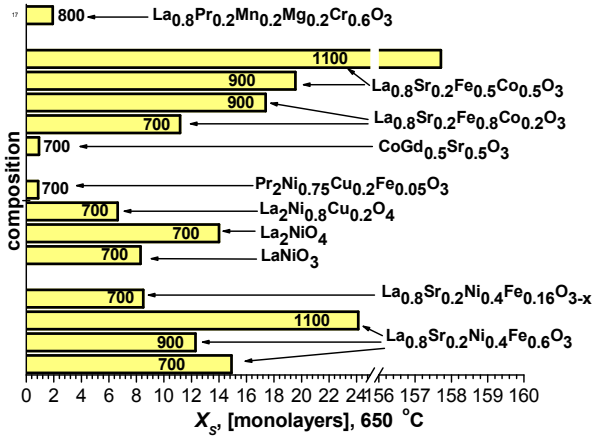

Figure 5. Dynamic degree of the oxygen heteroexchange at 650°C and 4 Torr O_2 versus samples composition and sintering temperature.

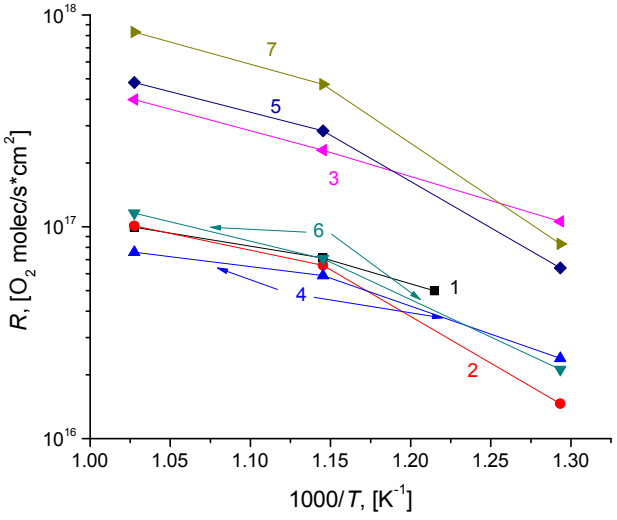

Figure 4. Typical temperature dependencies of specific rates of oxygen heteroexchange for perovskites and nanocomposites: $La_{0.8}Bi_{0.2}MnO_3$ sintered at 700°C (1), $La_{0.8}Bi_{0.2}MnO_3$ (50 wt. %) – $Bi_{1.5}Y_{0.3}Sm_{0.2}O_3$ sintered at 700°C (2) and 800°C (3), $La_{0.8}Bi_{0.2}MnO_3$ (30 wt. %) – $Bi_{1.5}Y_{0.3}Sm_{0.2}O_3$ sintered at 700°C (4) and 800°C (5), $La_{0.8}Bi_{0.2}MnO_3$ (70 wt. %) – $Bi_{1.5}Y_{0.3}Sm_{0.2}O_3$ sintered at 700°C (6) and 800°C (7) [59].

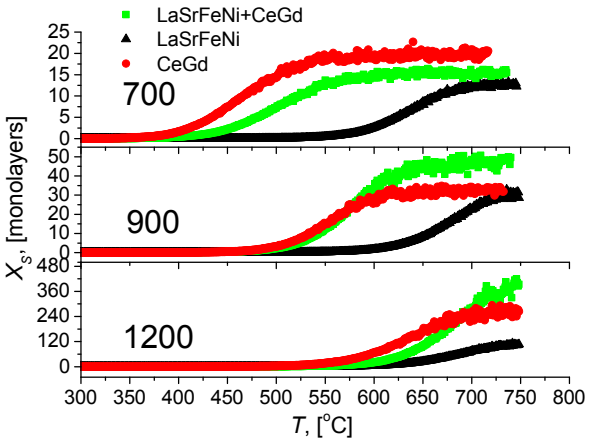

Figure 6. Effect of sintering temperature (700–1200°C) on dynamics of the oxygen heteroexchange at 4 Torr O_2 in the temperature-programmed mode on LSFN, GDC and LSFN–GDC nanocomposite.

in the intermediate-temperature range of SOFC operation ~700°C (Fig. 6). For both perovskites and perovskite-fluorite composites the increase of oxygen mobility with sintering temperature is explained by the increase of the length of the domain boundaries, which play the role of channels for fast oxygen diffusion [14-18]. Dynamic extent of exchange was shown to be extremely high for LSM-ScCeSZ nanocomposites significantly exceeding the values for LSM [17,18].

A detailed characterization of oxygen mobility in perovskites and perovskite-fluorite nanocomposites was achieved by fitting the plots of steady-state isotope transients (steady state isotopic transient kinetic analysis (SSITKA) method) [14]. The experimental data for GDC, perovskites, and Ruddlesden-Popper oxides are fitted by a simple model of a uniform oxygen diffusion in the bulk, considering that all oxygen in the bulk can be exchanged (Fig. 7).

For GDC-$LSFN_{0.3}$ nanocomposite, a satisfactory description was obtained only with a more complex model suggesting very fast oxygen exchange between the surface and perovskite-fluorite interfaces in the bulk of the composite particles (Fig. 8) [14]. This mobile oxygen can be rapidly exchanged with GDC domains and slower – with LSFN domains. As the rate-limiting step, the bulk oxygen diffusion can be considered only for perovskite phase domains, while for the GDC domains the rate of exchange is controlled by the surface reaction. Hence,

for GDC only the lower limits of the oxygen self-diffusion coefficients can be estimated (Table 1). In this case, the low-limit oxygen exchange diffusion coefficients are provided (Table 2). The parameters of the oxygen diffusion estimated in regard to the typical size of perovskite and fluorite domains and the amount of the mobile oxygen atoms located at the perovskite-fluorite interfaces are given in Table 1. The activation energy of the oxygen self-diffusion along the perovskite-fluorite interfaces is ~110 kJ mol^{-1}, which is close to that in GDC [2].

The low-limit values of average oxygen self-diffusion coefficients for perovskite-like oxides estimated by SSITKA are compared in Table 2. In agreement with the published data [36], for R-P type oxides the average D^* values are higher than those for perovskites. Though these values are lower than the values reported for dense ceramics estimated by SIMS [36], the trend of increasing D^* with sintering temperature is in agreement with variation of the dynamic extent of the exchange. This suggests that the domain boundaries in perovskites are the paths for the fast oxygen diffusion [60].

2.3.4 Dense ceramics

For dense perovskites and perovskite-fluorite composites, numerous studies on oxygen mobility and surface reactivity obtained by various techniques have been published. In a classical work on oxygen diffusion in $LaCoO_3$ single crystal [29], Ishigaki et al. demonstrated an agreement between the results obtained by SIMS Isotopic Exchange Depth Profile (IEDP) method and the gas-phase analysis of the oxygen isotope composition.

For dense polycrystalline ceramics, comparative data are difficult to obtain due to strong impact of the surface layer composition affected by pretreatment, gas phase impurities, segregation of the components, formation of surface scales, and interdiffusion [21-28]. For thin (~3000 Å) dense layers of La_2NiO_4 made by pulsed laser deposition, application of the electrical conductivity relaxation technique revealed existence of two regions with different exchange rates that correspond to two different microstructures [61]. The estimated k_{chem}. values differ by up to two orders of magnitude, while being at least 3 orders of magnitude lower than the values found for the dense ceramic samples. In any case, Co- and

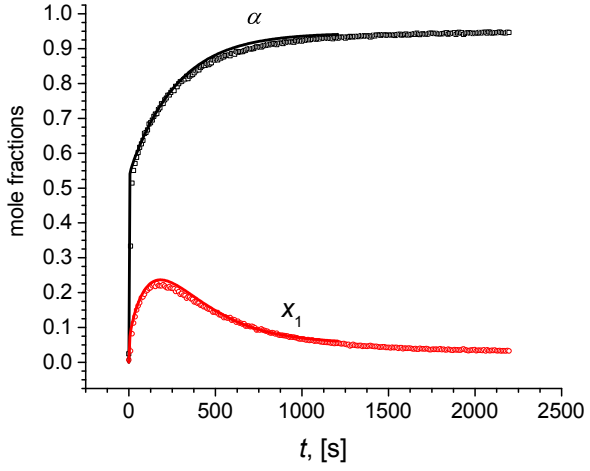

Figure 7. Typical variation of α and x_1 at the reactor exit after switch 1% $^{16}O_2$ in He → 1% $^{18}O_2$ in He at 700°C for Pr_2NiO_4 sample sintered at 1100°C. Points – experiment, lines – fitting using model with uniform lattice oxygen.

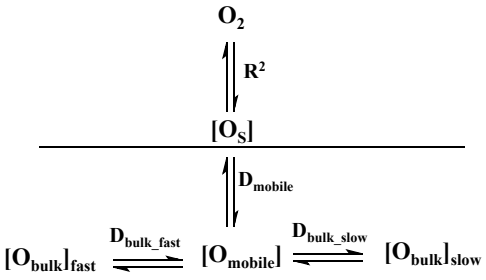

Figure 8. A heterogeneous model of oxygen exchange with GDC-$LSFN_{0.3}$ nanocomposite.

Table 1. The surface oxygen exchange constant k_{ex} (by R^2 mechanism) and coefficients of oxygen self-diffusion in the fluorite phase D_f, perovskite phase D_p and along interfaces $D_{interface}$ for LSFN-GDC nanocomposite.

T, [°C]	k_{ex}, [cm s^{-1}]	D_f, [cm^2 s^{-1}]	D_p, [cm^2 s^{-1}]	$D_{interface}$, [cm^2 s^{-1}]
600°C	1.4×10^{-8}	$\geq 6 \times 10^{-14}$	2×10^{-14}	$\geq 1 \times 10^{-8}$
700°C	3.6×10^{-8}	$\geq 30 \times 10^{-14}$	9×10^{-14}	$\geq 5 \times 10^{-8}$

Table 2. Characteristics of oxygen mobility and reactivity for powdered oxides by SSITKA.

Oxide/T sintering, [°C]	$T_{exchange}$, [°C]	k_{ex}, [cm s^{-1}]	D*, [cm^2 s^{-1}]
$LaMnO_3$ /1100 [59]	900	> 2.1 × 10^{-7}	4 × 10^{-12}
$La_{0.7}Sr_{0.3}MnO_{3\pm\delta}$/1100 [59]	900	> 3.9 × 10^{-7}	9 × 10^{-12}
$La_{0.7}Sr_{0.3}MnO_{3\pm\delta}$ /1100 [59]	800	> .6 × 10^{-7}	5 × 10^{-13}
$La_{0.4}Sr_{0.6}FeO_{3-\delta}$ /1100 [59]	800	9.1 × 10^{-8}	5 × 10^{-11}
$La_{0.8}Sr_{0.2}Fe_{0.7}Ni_{0.3}O_{3+\delta}$ /700	700		> 6 × 10^{-14}
$La_{0.4}Sr_{0.6}FeO_{3-\delta}$ [59]	800	9.1 × 10^{-8}	5 × 10^{-11}
Pr_2NiO_4 /1100	800	1.3 × 10^{-6}	> 8 × 10^{-10}
Pr_2NiO_4 /1100	600	2.7 × 10^{-7}	> 2 × 10^{-10}
Pr_2NiO_4 /900	600	2.7 × 10^{-7}	> 2 × 10^{-11}
Pr_2NiO_4 /700	600	6.7 × 10^{-8}	> 6 × 10^{-13}
La_2NiO_4/1100	800	2.3 × 10^{-7}	> 1 × 10^{-10}
La_2CuO_4/1000	800	3.4 × 10^{-8}	> 2 × 10^{-11}
$La_{0.4}Bi_{0.4}Sr_{0.2}MnO_x$/900	800	1.2 × 10^{-6}	> 1.3 × 10^{-10}
$La_{0.4}Bi_{0.4}Sr_{0.2}Fe_{0.5}Co_{0.5}O_x$/900	800	1.5 × 10^{-6}	> 3.0 × 10^{-10}

Ni-containing perovskites demonstrate a higher lattice oxygen mobility as compared to manganites (Table 3), which agrees with the data for the powder samples. For LFN perovskites with a high Ni content [62], the oxygen chemical diffusion coefficients are ~10^{-6} cm^2 s^{-1} in the temperature range of 650–850°C, which is promising for practical applications, especially in regard to their high stability and the ability of LFN to withstand presence of CO_2. The oxygen chemical exchange coefficients for LFN could strongly vary in dependence upon the mode of temperature, or oxygen partial pressure variation (jump up or jump down [62]) due to change of the surface layer oxygen stoichiometry, but they remainsufficiently high (Table 3). The chemical diffusion coefficients are higher for R-P phases than for perovskites (Table 3), demonstrating high efficiency of the cooperative route of oxygen diffusion via interstitials [40,41]. Partial substitution of Ni by Co in La_2NiO_4 increases k_{chem} but has small effect on D_{chem}. (Table 3) [33]. Among different Ln cations, Pr provides the highest oxygen mobility for the same composition, and Nd has the lowest [32]. Partial substitution of Ni by Fe or Cu in La_2NiO_4 results in decreasing both D_{chem} and k_{chem} [32], which agrees with the oxygen heteroexchange data for powders in static reactor (Figs. 2 and 5) and the conductivity relaxation data for La_2CuO_4 (Table 3).

Determining k_{chem} and D_{chem} values depends on the relation of domain size and characteristic size $LC^{(chem)} = D_{chem}/k_{chem}$. If the domain size is lower than L_C, surface exchange is limiting and diffusion coefficient is hard to determine. In the other case, diffusion is limiting. The same is also attributed to oxygen self-diffusion and surface exchange.

For layered perovskites such as $GdBaCo_2O_5$ [31], SIMS isotope exchange depth profiling (IEDP) demonstrates high oxygen mobility, which is only slightly lower than that for layered nickelates and agrees with the conductivity relaxation studies for BaSrCoFeO (BSCF) [7]. It is explained by a cooperative movement of oxide ions similar to that in R-P phases [45]. For composites, the SIMS studies reveal that an average oxygen self-diffusion coefficient increases as compared with perovskites [25]. The surface exchange coefficient is close to that in perovskites [25], which means that its non-additive increase is due to much lower activity of surface sites of electrolytes in activation of oxygen molecules [18]. For LSFC-GDC composites (30% GDC), comparative studies for dense ceramic pellets (SIMS and weight relaxation) and powders prepared by crushing and milling (oxygen isotope exchange in a static reactor) were carried out (Fig. 9) [18]. The values of the oxygen self-diffusion coefficient (D*) estimated by different methods (e.g. IEDP-SIMS [25], from fitting the exchange curves in a static reactor [18], or from the values of D_{chem} estimated by the weight relaxation method) and taking the same value for the thermodynamic factor for LSCF-GDC composite as for LSCF (~10^2) [27], are shown in Fig. 10. In general, all data are grouped along the line with the activation energy of ~150 kJ mol^{-1}, similar to that of LSCF [27, 28].

For LSFN-GDC perovskite–fluorite nanocomposite studied both as a powder and dense ceramics [14-16], the oxygen chemical diffusion coefficient increases with

Table 3. Characteristics of oxygen diffusion for dense ceramics

Materials	T, [K] / pO_2, [kPa]	logD*, [$cm^2\ s^{-1}$]	$logD_{chem}$, [$cm^2\ s^{-1}$]	$logk_{ex}$, [$cm\ s^{-1}$]	$logk_{chem}$, [$cm\ s^{-1}$]
La_2NiO_4 [26]	1223/21	-6.4	-4.6	-4.9	-3.1
La_2CuO_4 [26]	1223/21	-6.7	-4	-5	-2.4
Pr_2NiO_4 [32]	1000	-7		-6.2	
Nd_2NiO_4 [32]	1000	-7.3		-5.8	
$Nd_{1.8}Ca_{0.2}NiO_{4+\delta}$ [32]	1000	-8		-6.5	
$La_2Ni_{0.75}Cu_{0.25}O_{4+\delta}$ [32]	1000	-7.5		-5.8	
$La_{1.8}Sr_{0.2}NiO_{4+\delta}$ [32]	1000	-9		-7.2	
GBCO/CGO [31]	1000	-8.7		-5.9	
20% 0.4LSC+GDC [63]	1000	-7		-6.5	
50PNO+50GDC	1000/0.16		-3.7		-3.2
$LaFe_{0.7}Ni_{0.3}O_3$	1000/0.16		-6.3		
$50LaFe_{0.7}Ni_{0.3}O_3$+50GDC	973		-5		-3.5
$La_{0.6}Sr_{0.4}CoO_{3-\delta}$ [34]	1000/0.1		-7		-4.5
$La_{0.6}Sr_{0.4}Fe_{0.8}Co_{0.2}O_{3-\delta}$ [27]	1073/0.1	-7.2	-5.2	-6.5	-4.5
LSM [30]	1000	-15		-8.5	
La_2NiO_4 [33]	1000	-7.4		-6.5	
$La_2Ni_{0.5}Co_{0.5}O_4$ [33]	1000	-7.2		-5.7	
LSC [30]	1000	-10		-6.5	
$LaNi_{0.6}Fe_{0.4}O_3$ [61]	923-1123		-6		-3.8 – -4.8
$Bi_{0.5}Sr_{0.5}FeO_{3-\delta}$ [11]	1000		-3.5		-2.5
$La_{0.5}Sr_{0.5}FeO_{3-\delta}$ [11]	1000		-4.9		-3.8

*Variation of k_{chem} within an order of magnitude in two series of transient experiments with either decreasing or increasing temperature in a jump-one mode at a constant oxygen pressure [62].

the fraction of GDC by up to 1–1.5 orders of magnitude depending on the oxygen partial pressure (Figs. 11 and 12). The effect of the GDC addition is more pronounced at lower oxygen partial pressures, which suggests that fast oxygen migration along perovskite-fluorite interfaces is favoured by a partial reduction of GDC surface sites generating Ce^{3+} cations, and, hence, creating oxygen vacancies and increasing electronic conductivity. Higher values of k_{chem} and D_{chem} were obtained for LFN- GDC nanocomposites at higher temperatures (Fig. 13), while at lower temperatures (~ 700°C) the oxygen mobility is higher in LSFN-GDC nanocomposites [16,17]. Among other composites, the promising levels of oxygen mobility and reactivity were demonstrated for such systems as LSC/CGO [63], $PrNi_{0.6}Co_{0.4}O_3/Ce_{0.8}Sm_{0.2}O_{1.9}$ [19], LSM/YSZ [44], LSM/GDC [13], $La_{1.6}Sr_{0.4}NiO_{4+\delta}/Ce_{0.8}Sm_{0.2}O_{1.9}$, BSCF/GDC [64].

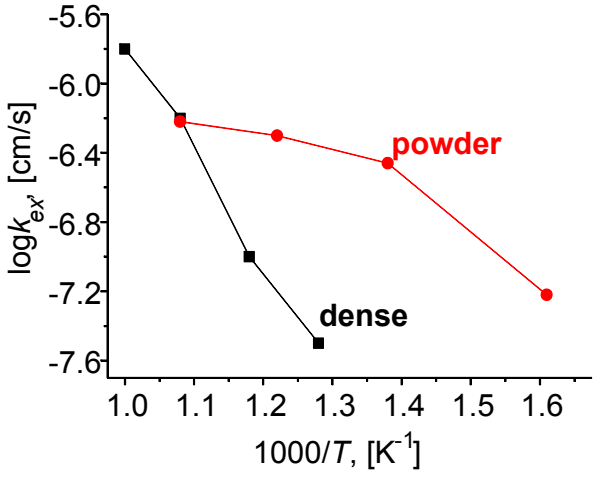

Figure 9. Comparison between coefficients of oxygen exchange in LSFC-GDC composite estimated for powders and dense material.

2.4 Performance

The most important characteristics of the cathode materials performance are the maximum power density and the cell polarization resistance. In the case of the anode-supported SOFCs fed by wet H_2 and air, the performance of different cathode materials can be compared. The composites of LSM with doped zirconia or ceria (Table 4; Fig. 14) provide a higher power density than LSM alone [65-67]. In this case the microstructure of the cathode layers and the

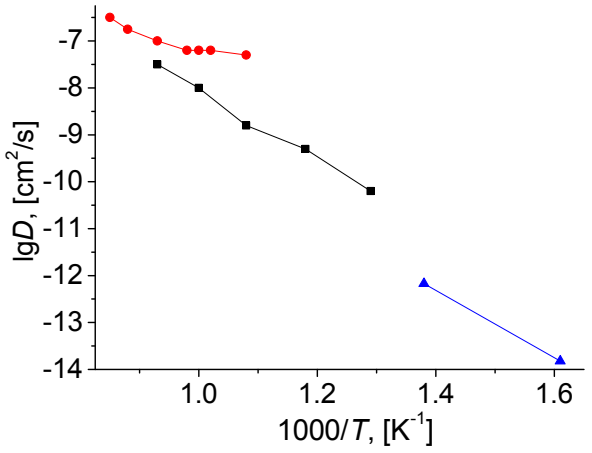

Figure 10. Comparison of oxygen self-diffusion coefficients for the pellet of LSFC-GDC composite estimated by SIMS [119] (squares), weight relaxation (circles) and isotope exchange in a static reactor (triangles) [64].

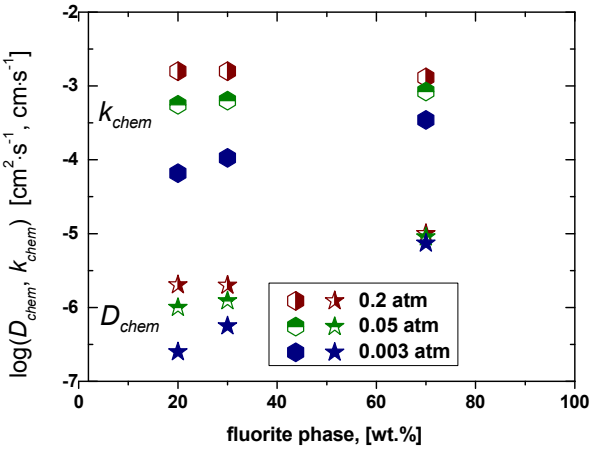

Figure 12. The effect of the fluorite phase content and oxygen partial pressure on D_{chem} and k_{chem} for nanocomposites (100-x)% LSFN – x% GDC at 700°C estimated by conductivity relaxation method.

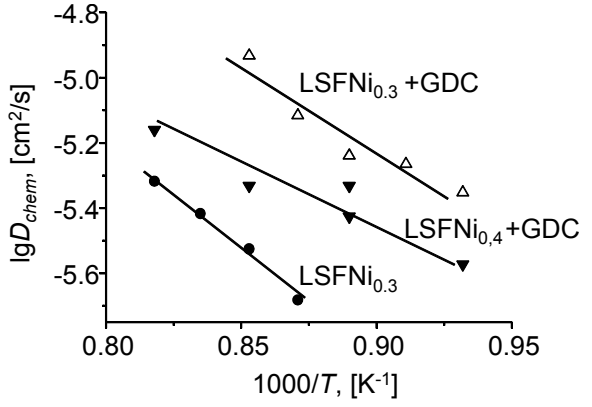

Figure 11. Temperature dependence of chemical diffusion coefficient estimated by weight relaxation method for dense pellets of composites and perovskites sintered at 1330°C.

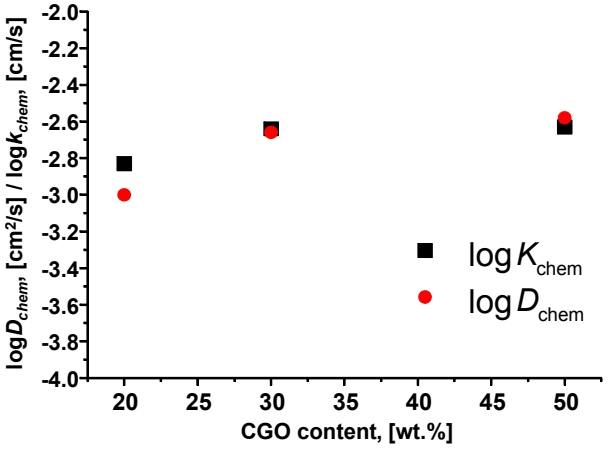

Figure 13. Oxygen chemical diffusion coefficient D_{chem} and chemical exchange constant k_{chem} vs. GDC content estimated by the weight relaxation method at 1050°C for LFN – CGO composite sintered at 1200°C.

nature/thickness of the electrolyte should be also taken into account [68]. Moreover, functionally graded cathode LSM/LSM+ScCeSZ on a thin layer of ScCeSZ electrolyte [65] provides even higher power density than LSCF perovskite well-known for its high lattice oxygen mobility and surface exchange rate [10]. Hence, the concept of a nanocomposite cathode material seems to be promising for design of thin film SOFCs operating at intermediate temperatures. Since at 750°C the power density of a cell with a LSCF cathode is high (Table 4) [69], it can be assumed that a lower power density for the cell with LSCF cathode at 600°C is due to segregation of Sr in the surface layer, thus blocking the surface sites [6]. Formation of carbonates cannot be excluded as well. Another type of perovskite cathode containing alkaline-earth cations – BSCF demonstrated a high power density (up to ~1 kWt cm^{-2}) at 600°C [8]. When BSCF-GDC composite is used along with a thin LSM interlayer between cathode and GDC electrolyte [70], the stability and power density of BSCF cathode at 600°C is improved (Table 4). Similarly, high and stable performance at 600°C was provided by functionally graded composite cathode 30% Co_3O_4 + 70% $Sm_{0.5}Sr_{0.5}CoO_{3-\delta}$ / 70% SDC + 30% $Sm_{0.5}Sr_{0.5}CoO_{3-\delta}$ [71] (Table 4). This suggests that composite cathodes possess high oxygen mobility and surface reactivity and also a higher resistance to poisoning by surface carbonates. The $La_{0.99}Co_{0.4}Ni_{0.6}O_{3-\delta}$ - $Ce_{0.9}Gd_{0.1}O_{1.95}$

Table 4. Max power density of single button-size SOFC with different cathodes.

Cell/[Reference]	T, °C	Power density, mW cm^{-2}
LSM (5mm)/YSZ (20mm)/Ni-YSZ [64]	850	120
LSM (~50mm)/ScCeSZ (~5mm)/Ni-YSZ [68]	800	450
LSM/LSM+ScCeSZ (~20mm)/ScCeSZ (~5mm)/Ni-YSZ [65]	800	1250
	600	300
LSM+YSZ (~50mm)/ YSZ (10mm)/Ni-YSZ (2mm) [65]	800	800
LSM (50mm)/ YSZ (30mm)/Ni-YSZ (1mm) [66]	700	50
LSM+YSZ (~50mm)/ YSZ (30mm)/Ni-YSZ (1mm)	700	200
LSM+SDC (~50mm)/ YSZ (30mm)/Ni-YSZ (1mm)	700	400
	600	200
Pr_2NiO_4 /1.3mm GDC/ 3–5mm 8YSZ/NiYSZ [10]	600	400
LSCF/1.3mm GDC// 3–5mm 8YSZ/NiYSZ [10]	600	184
$La_{0.6}Sr_{0.4}Co_{0.2}Fe_{0.8}O_3$ (13 mm)/SDC(4 mm)/ YSZ (6mm)/ Ni-YSZ (50/50 vol%) [67]	750	1000
$Ba_{0.5}Sr_{0.5}Co_{0.8}Fe_{0.2}O_{3-\delta}$ (~20 mm)/ $Sm_{0.15}Ce_{0.85}O_{2-\delta}$ (~20 mm)/Ni +$Sm_{0.15}Ce_{0.85}O_{2-\delta}$ (~700 mm) [8]	600	
Pure O_2		900
O_2 +1%CO_2		650
$Ba_{0.5}Sr_{0.5}Co_{0.8}Fe_{0.2}O_{3-\delta}$ – 30%GDC/LSM/GDC (20 mm)/Ni-GDC [69]	600	1000
30%Co_3O_4+70%$Sm_{0.5}Sr_{0.5}CoO_{3-\delta}$ (100 mm) /70%SDC+30%SSC (30 mm)/ SDC (25 mm)/Ni-GDC [70]	600	1080
$La_{0.99}Co_{0.4}Ni_{0.6}O_{3-\delta}$ – $Ce_{0.9}Gd_{0.1}O_{1.95}$ /GDC/ ScYSZ/Ni-ScYSZ [71]	750	1200
$PrNi_{0.6}Co_{0.4}O_3$ +50% $Ce_{0.8}Sm_{0.2}O_2$/ SDC (10 mm) /Ni+SDC [19]	700	1090
La_2NiO_4/ SDC (200 mm) /Ni+ SDC [9]	800	150
La_2NiO_4 + SDC (2:1)/ SDC (200 mm) /Ni+SCeO [9]	800	450
50 $Bi_2Ru_2O_7$: 50 ESB/ESB (5 mm)/GDC (10 mm)/Ni-GDC [73]	650	2000
$Bi_{0.5}Sr_{0.5}FeO_{3-\delta}$ /SDC (2 mm)/YSZ (6 mm)/ YSZ/Ni (50/50 vol%) [11]	750	1100

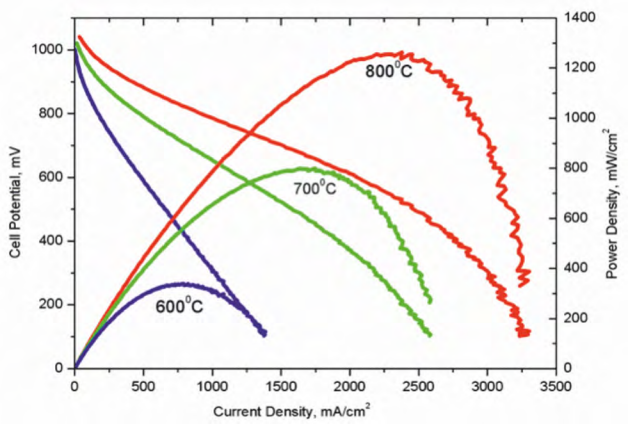

Figure 14. Potential and power density vs. current density curves for cell with a thin layer of YSZ electrolyte supported by MO CVD and functionally graded LSM/LSM+ScCeSZ cathode [65].

[72] and $PrNi_{0.6}Co_{0.4}O_3$ + 50% $Ce_{0.8}Sm_{0.2}O_2$ composites [19] without alkaline-earth cations provide high power density at 700°C and should be also resistant to formation of surface carbonate layers. Nanocomposite of R-P La_2NiO_4 phase with SDC electrolyte [9] provides a higher power density than La_2NiO_4 alone due to decreased polarization resistance. Relatively low power density obtained in this work for the cells with La_2NiO_4 (despite high oxygen mobility and surface reactivity) is explained by a thick SDC electrolyte layer, and high ohmic resistance of the cell. Application of Bi-containing electrolytes could cause some additional problems due to BiO_x volatility during sintering. In this respect, a high power density provided by $Bi_{0.5}Sr_{0.5}FeO_{3-\delta}$ cathode supported on binary thin film electrolyte SDC/YSZ [21] should be considered (Table 4).

3 Conclusions

A reasonable agreement between the results obtained by different techniques focused on oxygen mobility and surface reactivity (e.g. oxygen isotope exchange, and weight and conductivity relaxation) for several selected systems has been demonstrated. The morphology of the surface and the bulk of the cathode materials based on perovskite-like phases and their nanocomposites with fluorite-like electrolytes (doped ceria or zirconia) play a significant role in comparison to their chemical composition and lattice arrangement in controlling the oxygen mobility and surface reactivity. In nanocomposites, an enhanced oxygen mobility along perovskite – fluorite interfaces and generation of new active sites for oxygen exchange on the surface of the electrolyte domains due to migration of transition metal cations makes these systems

attractive for design of IT SOFC cathodes. Nanocomposites of doped ceria with mixed nickelate-cobaltites or ferrites of Pr (without alkaline-earth metal cations) possess high stability to degradation caused by CO_2 and H_2O in air, thus being promising for SOFC operation at decreased (600–700°C) temperatures.

Acknowledgements: Support of this research by International projects (NATO SFP 980878, SOFC 600, MATSILC, Russian-German Project N-Cath of CLIENT Program) and Russian projects (Integration Projects of SB RAS 95, 57 and 8; Project of Presidium RAS 50, Federal Program "Scientific and Educational Cadres of Russia") is gratefully acknowledged.

List of Symbols

D_{chem} – chemical diffusion coefficient
D^* – oxygen self-diffusion coefficient
k_{chem} – chemical exchange constant
k_{ex} – oxygen surface exchange constant
R – specific rate of oxygen heteroexchange
x_1 – $^{16}O^{18}O$ (or $C^{16}O^{18}O$) molecules fraction
x_2 –$^{18}O_2$ (or $C^{18}O_2$) molecules fraction
X_S – dynamic extent of exchange
α – ^{18}O atoms fraction
σ – overall electrical conductivity
σ_i – ionic conductivity

References

[1] Wincewicz K., Cooper J., Taxonomies of SOFC Material and Manufacturing Alternatives, Journal of Power Sources, 2005, 140, 280-296.
[2] Steele B.C.H., Materials for IT-SOFC Stacks 35 years R&D: the Inevitability of Gradualness, Solid State Ionics, 2000, 134, 3-20.
[3] Adler S.B., Factors Governing Oxygen Reduction in Solid Oxide Fuel Cell Cathodes, Chemical Reviews, 2004, 104, 4791-4843.
[4] Mitterdorfer A., Gauckler L.J., Mechanism of $La_2Zr_2O_7$ (LZ) Formation at the LSM/YSZ Single-Crystal Interface Based on HRTEM and AFM Measurements, Solid State Ionics, 1998, 111, 185.
[5] Yang M., Bucher E., Sitte W., Effects of Chromium Poisoning on the Long-term Oxygen Exchange Kinetics of the Solid Oxide Fuel Cell Cathode Materials $La_{0.6}Sr_{0.4}CoO_3$ and Nd_2NiO_4, Journal of Power Sources, 2011, 196, 7313-7317.
[6] Bucher E., Sitte W., Long-term Stability of the Oxygen Exchange Properties of $(La,Sr)_{1-z}(Co,Fe)O_{3-\delta}$ in Dry and Wet Atmospheres, Solid State Ionics, 2011, 192, 480-482.
[7] Zhou W., Ran R., Shao Z., Progress in Understanding and Development of $Ba_{0.5}Sr_{0.5}Co_{0.8}Fe_{0.2}O_{3-\delta}$-based Cathodes for Intermediate-Temperature Solid-Oxide Fuel Cells: A review, Journal of Power Sources, 2009, 192, 231-246.
[8] Li Y., Yang M., Hou Zh., Dong Y., Cheng M., Investigation of $Ba_{1-x}Sr_xCo_{0.8}Fe_{0.2}O_{3-\delta}$ as Cathodes for Low-Temperature Solid Oxide Fuel Cells Both in the Absence and Presence of CO_2, Journal of Power Sources, 2008, 185, 76-84.
[9] Pérez-Coll D., Aguadero A., Escudero M.J., Núñez P., Daza L., Optimization of the Interface Polarization of the La_2NiO_4-based Cathode Working with the $Ce_{1-x}Sm_xO_{2-\delta}$ Electrolyte System, Journal of Power Sources, 2008, 178, 151-162.
[10] Ferchaud C., Grenier J.-C., Zhang-Steenwinkel Y., van Tuel M.M.A., van Berkel F. P.F., Bassat J.-M., High Performance Praseodymium Nickelate Oxide Cathode for Low Temperature Solid Oxide Fuel Cell, Journal of Power Sources, 2011, 196, 1872-1879.
[11] Niu Y., Zhou W., Sunarso J., Ge L., Zhu Zh., Shao Z., High Performance Cobalt-Free Perovskite Cathode for Intermediate Temperature Solid Oxide Fuel Cells, Journal of Materials Chemistry, 2010, 20, 9619-9622.
[12] Kenjo T., Nishiya M., $LaMnO_3$ Air Cathodes Containing ZrO_2 Electrolyte for High Temperature Solid Oxide Fuel Cells, Solid State Ionics, 1992, 57, 295-302.
[13] Murray E.P., Barnett S.A., Improved Performance in $(La,Sr)MnO_3$ and $(La,Sr)(Co,Fe)O_3$ Cathodes by the Addition of a Gd-doped Ceria Second Phase, In: S.C. Singhal, M. Dokiya (Eds.), Proceedings of the Sixth International Symposium on Solid Oxide Fuel Cells (SOFC VI) (17-22 June 1999, Honolulu, USA), The Electrochemical Society, 1999, 199.
[14] Sadykov V., Mezentseva N., Usoltsev V., Sadovskaya E., Ishchenko A., Pavlova S., Bespalko Yu., Kharlamova T., Zevak E., Salanov A., Krieger T., Bobrenok O., Uvarov N., Okhlupin Yu., Smorygo O., Smirnova A., Singh P., Vlasov A., Korobeynikov M., Bryazgin A., Kalinin P., Arzhannikov A., SOFC Composite Cathodes Based on Perovskite and Fluorite Structures, Journal of Power Sources, 2010, 196, 7104-7109.
[15] Kharlamova T., Pavlova S., Sadykov V., Bespalko Y., Krieger T., Pelipenko V., Belyaev V., Muzykantov V., Alikina G., Okhlupin Y., Uvarov N., Smirnova A., Nanocomposite Cathode Materials for Intermediate Temperature Solid Oxide Fuel Cells, ECS Transactions, 2011, 35, 2331-2340.
[16] Pavlova S., Kharlamova T., Savykov V., Krieger T., Muzykantov V., Bespalko Yu., Ishchenko A., Rogov V., Belyaev V., Okhlupin Y., Uvarov N., Structural Features and Transport Properties of $La(Sr)Fe_{1-x}Ni_xO_{3-\delta}$ – $Ce_{0.9}Gd_{0.1}O_{2-\delta}$ Nanocomposites, In: B.B. Saha, A. Chakraborty, K.Ng Choon (Eds.). Innovative Materials for Processes in Energy Systems, IMPRES, 2010, 128-135.
[17] Sadykov V., Alikina G., Lukashevich A., Muzykantov V., Usoltsev V., Boronin A., Koscheev S., Krieger T., Ishchenko A., Smirnova A., Bobrenok O., Uvarov N., Design and Characterization of LSM/ScCeSZ Nanocomposite As Mixed Ionic-Electronic Conducting Material For Functionally Graded Cathodes Of Solid Oxide Fuel Cells, Solid State Ionics, 2011, 192, 540-546.
[18] Sadykov V.A., Pavlova S.N., Kharlamova T.S., Muzykantov V.S., Uvarov N.F., Okhlupin Yu.S., Ishchenko A.V., Bobin A.S., Mezentseva N.V., Alikina G.M., Lukashevich A.I., Krieger T.A., Larina T.V., Bulgakov N.N., Tapilin V.M., Belyaev V.D., Sadovskaya E.M., Boronin A.I., Sobyanin V.A., Bobrenok O.F., Smirnova A.L., Smorygo O.L., Kilner J.A., Perovskites and Their Nanocomposites with Fluorite-Like Oxides as Materials for Solid Oxide Fuel Cells Cathodes and Oxygen-Conducting

Membranes: Mobility and Reactivity of the Surface/Bulk Oxygen as a Key Factor of Their Performance, In: M. Borowski (Ed.), Perovskites: Structure, Properties and Uses, Nova Science Publishers, Inc, 2010, 67-178.

[19] Huang S., Lu Q., Feng S., Li G., Wang C., $PrNi_{0.6}Co_{0.4}O_3$–$Ce_{0.8}Sm_{0.2}O_{1.9}$ Composite Cathodes for Intermediate Temperature Solid Oxide Fuel Cells, Journal of Power Sources, 2012, 199, 150-154.

[20] Armstrong T., Virkar A., Performance of Solid Oxide Fuel Cells with LSGM-LSM Composite Cathodes, Journal of the Electrochemical Society, 2002, 149(12), A1565-A1571.

[21] Diethelm S., Closset A., Van herle J., McEvoy A.J., Nisancioglu K., Study of Oxygen Exchange and Transport in Mixed Conducting Cobaltites by Electrochemical Impedance Spectroscopy, Solid State Ionics, 2000, 135, 613-618.

[22] Sunde S., Nisancioglu K., Gur T.M., Critical Analysis of Potentiostatic Step Data for Oxygen Transport in Electronically Conducting Perovskites, Journal of the Electrochemical Society, 1996, 143, 3497–3504.

[23] Lankhorst M.H.R., Bouwmeester H.J.M., Determination of Oxygen Nonstoichiometry and Diffusivity in Mixed Conducting Oxides by Oxygen Coulometric Titration I: Chemical Diffusion in $La_{0.8}Sr_{0.2}CoO_{3-\delta}$, Journal of the Electrochemical Society, 1997, 144, 1261-1267.

[24] Chater R.J., Carter S., Kilner J.A., Steele B.C.H. Development of a Novel SIMS Technique for Oxygen Self-Diffusion and Surface Exchange Coefficient Measurements in Oxides of High Diffusivity, Solid State Ionics, 1992, 53-56, 859-867.

[25] Esquirol A., Kilner J., Brandon N., Oxygen Transport in $La_{0.6}Sr_{0.4}Co_{0.2}Fe_{0.8}O_{3-\delta}/Ce_{0.8}Gd_{0.2}O_{2-x}$ Composite Cathode for IT-SOFCs // Solid State Ionics, 2004, 175, 63-67.

[26] Kusnezoff M., Ziesche S., Elschner Ch., Measurement of Chemical Diffusion Coefficient and Surface Exchange on Mixed Ionic Electronic Conductors Using Periodical pO_2 Oscillations, Journal of Membrane Science, 2010, 360, 9-16.

[27] Katsuki M., Wang Sh., Dokiya M., Hashimoto T., High Temperature Properties of $La_{0.6}Sr_{0.4}Co_{0.8}Fe_{0.2}O_{3-\delta}$: Oxygen Nonstoichiometry and Chemical Diffusion Constant, Solid State Ionics, 2003, 156, 453-461.

[28] Lane J.A., Benson S.J., Waller D., Kilner J.A., Oxygen Transport in $La_{0.6}Sr_{0.4}Co_{0.2}Fe_{0.8}O_{3-\delta}$, Solid State Ionics, 1999, 121, 201-208.

[29] Ishigaki T., Yamaguchi Sh., Mizusaki J., Fueki K., Tracer Diffusion Coefficient of Oxide Ions in $LaCoO_3$ single Crystal, Journal of Solid State Chemistry, 1984, 54, 100-107.

[30] De Souza R.A., Kilner J.A., Oxygen Transport in La-Sr- Mn-Co-O Perovskites, Solid State Ionics, 1999, 126, 153-161.

[31] Parfitt D., Chroneos A., Tarancon A., Kilner J.A., Oxygen Ion Diffusion in Cation Ordered/Disordered $GdBaCo_2O_{5+\delta}$, Journal of Materials Chemistry, 2011, 21, 2183-2186.

[32] Boehm E., Bassat J.-M., Dordor P., Mauvy F., Grenier J.-C., Stevens Ph., Oxygen Diffusion and Transport Properties in Non-Stoichiometric $Ln_{2-x}NiO_{4+\delta}$ oxides, Solid State Ionics, 2005, 176, 2717-2725.

[33] Kilner J.A., Shaw C.K.M., Mass Transport in $La_2Ni_{1-x}Co_xO_{4+\delta}$ Oxides with the K_2NiF_4 Structure, Solid State Ionics, 2002, 154-155, 523-527.

[34] Kan C.C., Wachsman E.D., Isotopic-Switching Analysis of Oxygen Reduction in Solid Oxide Fuel Cell Cathode Materials, Solid State Ionics, 2010, 181, 338-347.

[35] Benson S.J., Chater R.J., Kilner J.A., Oxygen Diffusion and Surface Exchange in the Mixed Conducting Perovskite $La_{0.6}Sr_{0.4}Fe_{0.8}Co_{0.2}O_{3-\delta}$, In: T.A. Ramanarayanan (Ed.), Electrochemical Society Proceedings, Ionic and Mixed Conducting Ceramics III, ECS, Pennington, NJ, 1998, 97-24, 596-609.

[36] Li Z., Haugsrud R., Effects of Surface Coatings on the Determination of D_{chem} and k_{chem} in $La_2NiO_{4+\delta}$ by Conductivity Relaxation, Solid State Ionics, 2012, 206, 67-71.

[37] Shaw C.K.M., Kilner J.A., Skinner S.J., Mixed Cobalt and Nickel Containing Perovskite Oxide for Intermediate Temperature Electrochemical Applications, Solid State Ionics, 2000, 135, 765-769.

[38] Ishigaki T., Yamauchi Sh., Kishio K., Mizusaki J., Fueki K., Diffusion of Oxide Ion Vacancies in Perovskite-Type Oxides, Journal of Solid State Chemistry, 1988, 73, 179-187.

[39] Islam M.S., Computer Modelling of Defects and Transport in Perovskite Oxides, Solid State Ionics, 2002, 154-155, 75-85.

[40] Read M.S.D., Islam M.S., Watson G.W., Hancock F.E., Surface Structures and Defect Properties of Pure and Doped La_2NiO_4, Journal of Materials Chemistry, 2001, 11, 2597-2602.

[41] Allan N.L., Mackrodt W.C., Oxygen Ion Migration in La_2CuO_4, Philosophical Magazine, 1991, 64, 1129-1132.

[42] Cai Z., Kubicek M., Fleig J., Yildiz B., Chemical Heterogeneities on $La_{0.6}Sr_{0.4}CoO_{3-\delta}$ Thin Films: Correlations to Cathode Surface Activity and Stability, Chemistry of Materials, 2012, 24, 1116-112.

[43] Steele B.C.H., Bae J.-M., Properties of $La_{0.6}Sr_{0.4}Co_{0.2}Fe_{0.8}O_{3-x}$ (LSCF) Double Layer Cathodes on Gadolinium-doped Cerium Oxide (CGO) Electrolytes: II. Role of Oxygen Exchange and Diffusion, Solid State Ionics, 1998, 106, 255-261.

[44] Steele B.C.H., Hori K.M., Uchino S., Kinetic Parameters Influencing the Performance of IT-SOFC Composite Electrodes, Solid State Ionics, 2000, 135, 445-450.

[45] Burriel M., Pena-Martinez J., Chater R.J., Fearn S., Berenov A.V., Skinner S.J., Kilner J.A., Anisotropic Oxygen Ion Diffusion in Layered $PrBaCo_2O_{5+\delta}$ // Chemistry of Materials, 2012, 24(3), 613-621.

[46] Burriel M., Garcia G., Santiso J., Kilner J.A., Chater R.J., Skinner S.J., Anisotropic Oxygen Diffusion Properties in Epitaxial Thin Films of $La_2NiO_{4+\delta}$ // Journal of Materials Chemistry, 2008, 18, 416-422.

[47] Kim G., Wang S., Jacobson A.J., Chen C.L., Measurement of Oxygen Transport Kinetics in Epitaxial $La_2NiO_{4+\delta}$ Thin Films by Electrical Conductivity Relaxation, Solid State Ionics, 2006, 177, 1461-1467.

[48] Sadykov V.A., Kharlamova T.S., Mezentseva N.V., Pavlova S.N., Sadovskaya E.M., Muzykantov V.S., Bespalko Yu.N., Usol'tsev V.V., Zevak E.G., Kriger T.A., Ishchenko A.V., Uvarov N.F., Ulikhin A.S., Chaikina M.V., Argirusis C., Studies of Oxygen Transport Mechanism in Electrolytes Based on Doped Lanthanum Silicate with Apatite Structure Using Techniques of Oxygen Isotopic Heteroexchange and Impedance Spectroscopy, Russian Journal of Electrochemistry, 2011, 47(4), 427-441.

[49] De Souza R.A., A Universal Empirical Expression for the Isotope Surface Exchange Coefficients (k*) of Acceptor-doped Perovskite and Fluorite Oxides, Physical Chemistry Chemical Physics, 2006, 8, 890-897.

[50] Adler S.B., Chen X.Y., Wilson J.R., Mechanisms and Rate Laws for Oxygen Exchange on Mixed-Conducting Oxide Surfaces, Journal of Catalysis, 2007, 245, 91-109.

[51] Kharton V.V., Yaremchenko A.A., Naumovich E.N., Research on the Electrochemistry of Oxygen Ion Conductors in the Former Soviet Union. II. Perovskite-Related Oxides, Journal of Solid State Electrochemistry, 1999, 3, 303-326.

[52] Ullman H., Trofimenko N., Tietz F., Stöver D., Ahmad-Khanlou A., Correlation Between Thermal Expansion and Oxide Ion Transport in Mixed Conducting Perovskite-type Oxides for SOFC Cathodes, Solid State Ionics, 2000, 138, 79-90.

[53] Sakai N., Kishimoto H., Yamaji K., Horita T., Brito M.E., Yokokawa H., Interface Stability of Perovskite Cathodes and Rare-Earth Doped Ceria Interlayer in SOFCs, Journal of The Electrochemical Society, 2007, 154, B1331-B1337.

[54] Kim G.T., Jacobson, A.J., Electrochemical Characterization of $La_{2-x}Pr_xNiO_{4+x}$ for Application as Cathodes in Intermediate temperature SOFCs, Materials Research Society Symposium Proceedings, 2007, 972, 175-180.

[55] Sadykov V., Pavlova S., Zarubina V., Bobin A., Alikina G., Lukashevich A., Muzykantov V., Usoltsev V., Kharlamova T., Boronin A., Koscheev S., Krieger T., Ishchenko A., Mezentseva N., Salanov A., Smirnova A., Bobrenok O., Uvarov N., Design and Characterization of Functionally Graded Cathode Materials for Solid Oxide Fuel Cells, ECS Transactions, 2009, 25, 2403-2412.

[56] Angoua B.F., Slamovich E.B., Single Solution Spray Pyrolysis of $La_{0.6}Sr_{0.4}Co_{0.2}Fe_{0.8}O_{3-\delta}$ – $Ce_{0.8}Gd_{0.2}O_{1.9}$ (LSCF–CGO) Thin Film Cathodes, State Ionics, 2012, 212, 10-17.

[57] Sadykov V., Borchert Yu., Alikina G., Lukashevich A., Bunina R., Zabolotnaya G., Mezentseva N., Moroz E., Zaikovskii V., Zyuzin D., Uvarov N., Zyryanov V., Orlovskaya N., One-Pot Synthesis Of Mixed Ionic-Electronic Conducting Nanocomposites Comprised Of Fluorite-Like And Perovskite-Like Phases As Catalytic Materials For SOFC, In: C. Schatz, R.P. Van Duyne (Eds.), Materials Research Society Symposium Proc. (27 November – 1 December 2006, Boston), Boston, MA, 2006, 900E, O10.08.1-6.

[58] Zyryanov V.V., Sadykov V.A., Ivanovskaya M.I., Criado J.M., Neophytides S., Synthesis And Sintering Of Ceramic Nanocomposites With High Mixed Conductivity, Science of Sintering, 2005, 37, 45-54.

[59] Sadykov V., Mezentseva N., Arapova M., Krieger T., Gerasimov E., Alikina G., Pelipenko V., Bobin A., Muzykantov V., Fedorova Y., Sadovskaya E., Eremeev N., Belyaev V., Okhlupin Y., Uvarov N., Fast oxygen transport in bismuth oxide containing nanocomposites, Solid State Ionics, 2013, 251, 34-39.

[60] Ivanov D.V., Activity Of Perovskite-Like Oxides $La_{1-x}Sr_x(Mn,Fe)O_{3\pm\delta}$ (x=0-0.7) and $(La_{1-y}Sr_y)_2(Mn,Fe)O_{4\pm\delta}$ In High-Temperature Reactions Of Nitrous Oxide Decomposition And Methane Oxidation. Effect Of Oxygen Mobility. PhD Thesis, Boreskov Institute of Catalysis, Novosibirsk, Russia, 2012.

[61] Kim G., Wang S., Jacobson A.J., Chen C.L., Measurement Of Oxygen Transport Kinetics In Epitaxial La2NiO4+δ Thin Films By Electrical Conductivity Relaxation, Solid State Ionics, 2006, 177, 1461-1467.

[62] Chen J.Y., Rebello J., Vashook V., Trots D.M., Wang Sh.R., Wen T.L., Zosel J., Guth U., Thermal Stability, Oxygen Non-Stoichiometry And Transport Properties of $LaNi_{0.6}Fe_{0.4}O_3$, Solid State Ionics, 2011, 192, 424-430.

[63] Seeharaj P., Berenov A., Raj E., Rudkin R., Atkinson A., Mixed-conducting LSC/CGO Composites For Passive Oxygen Separation Membranes, Solid State Ionics, 2011, 192, 638-641.

[64] Yoon J.S., Yoon M.Y., Lee E.J., Moon J.-W., Hwang H.J., Influence of $Ce_{0.9}Gd_{0.1}O_{2-\delta}$ particles on microstructure and oxygen permeability of $Ba_{0.5}Sr_{0.5}Co_{0.8}Fe_{0.2}O_{3-\delta}$ composite membrane, Solid State Ionics, 2010, 181, 1387-1393.

[65] Charpentier P., Fragnaud P., Schleich D.M., Gehain E., Preparation of Thin Film SOFCs working at reduced temperature, Solid State Ionics, 2000, 135, 373-380.

[66] Sadykov V.A., Mezentseva N.V., Usoltsev V.V., Kharlamova T.S., Pavlova S.N., Belyaev V.D., Alikina G.M., Bunina R.V., Pelipeko V.V., Bobrova L.N., Ishchenko A.V., Bobrenok O.F., Uvarov N.F., Okhlupin Yu.S., Bronin D.I., Beresnev S.M., Bogdanovich N.M., Kuzin B.L., Kurteeva A.A., Smorygo O.L., Mikutski V.A., Smirnova A.L., Korobeinikov M.V., Arzhannikov A.V., Singh P., Rietveld B., van Berkel F., Planar Thin Film Solid Oxide Fuel Cells for Intermediate Temperature Operation (IT SOFC): Design and Performance // In: Zh. Liu (Ed.), Fuel Cell Performance, NY: Nova Science Publishers, 2012, 143-210.

[67] Chervin Ch., Glass R.S., Kauzlarich S.M., Chemical degradation of $La_{1-x}Sr_xMnO_3/Y_2O_3$-stabilized ZrO_2 composite cathodes in the presence of current collector pastes, Solid State Ionics, 2005, 176, 17-23.

[68] Yoon S.P., Han J., Nam S.W., Lim T.-H., Oh I.-H., Hong S.-A., Yoo Y.-S., Lim H.Ch., Performance of anode-supported solid oxide fuel cell with $La_{0.85}Sr_{0.15}MnO_3$ cathode modified by sol–gel coating technique, Journal of Power Sources, 2002, 106, 160-166.

[69] Lu Z., Hardy J., Templeton J., Stevenson J., Extended Reaction Zone of $La_{0.6}Sr_{0.4}Co_{0.2}Fe_{0.8}O_3$ Cathode For Solid Oxide Fuel Cell, J. Power Sources, 2012, 198, 90-94.

[70] Yang M., Zhang M., Yan A., Yue X., Hou Zh., Dong Y., Cheng M., Interaction of $La_{0.8}Sr_{0.2}MnO_3$ Interlayer With $Gd_{0.1}Ce_{0.9}O_{1.95}$ Electrolyte Membrane and $Ba_{0.5}Sr_{0.5}Co_{0.8}Fe_{0.2}O_{3-\delta}$ Cathode In Low-Temperature Solid Oxide Fuel Cells, J. Power Sources, 2008, 185, 784-789.

[71] Zhang H., Liu H., Cong Y., Yang W., Investigation of $Sm_{0.5}Sr_{0.5}CoO_{3-\delta}/Co_3O_4$ composite cathode for intermediate-temperature solid oxide fuel cells, Journal of Power Sources, 2008, 185, 129-135.

[72] Hjalmarsson P., Mogensen M., $La_{0.99}Co_{0.4}Ni_{0.6}O_{3-\delta}$ – $Ce_{0.8}Gd_{0.2}O_{1.95}$ as Composite Cathode For Solid Oxide Fuel Cells, J. Power Sources, 2011, 196, 7237-7244.

[73] Wachsman E.D., Development of a Lower Temperature SOFC, ECS Transactions, 2009, 25, 783-788.